

**Vertical extent of  
nucleation events**

J. Boulon et al.

This discussion paper is/has been under review for the journal Atmospheric Chemistry and Physics (ACP). Please refer to the corresponding final paper in ACP if available.

# Investigation of nucleation events vertical extent: a long term study at two different altitude sites

J. Boulon<sup>1</sup>, K. Sellegri<sup>1</sup>, M. Hervo<sup>1</sup>, D. Picard<sup>1</sup>, J.-M. Pichon<sup>1</sup>, P. Freville<sup>1</sup>, and P. Laj<sup>2</sup>

<sup>1</sup>Laboratoire de Météorologie Physique CNRS UMR 6016, Observatoire de Physique du Globe de Clermont-Ferrand, Université Blaise Pascal, France

<sup>2</sup>Laboratoire de Glaciologie et Géophysique de l'Environnement, CNRS UMR5183, Saint Martin d'Hères, France

Received: 17 February 2011 – Accepted: 7 March 2011 – Published: 10 March 2011

Correspondence to: J. Boulon (j.boulon@opgc.univ-bpclermont.fr)

Published by Copernicus Publications on behalf of the European Geosciences Union.

Title Page	
Abstract	Introduction
Conclusions	References
Tables	Figures
◀	▶
◀	▶
Back	Close
Full Screen / Esc	
Printer-friendly Version	
Interactive Discussion	



## Abstract

In this work we present an analysis of the occurrence of nucleation events during more than three years of measurements at two different rural altitude sites, the puy de Dôme research station (1465 m a.s.l.) and the Opme station (660 m a.s.l.), central France. The collected database is a unique combination of a Scanning Mobility Particle Sizer (SMPS, 10–400 nm) measurements, an air ion spectrometers (AIS, 0.5 to 45 nm) and neutral clusters and air ion spectrometers (NAIS, 0.5 to 45 nm) measurements at two different altitudes nearly located research stations, from February 2007 to June 2010. During the measurement period, neither the particle formation rates ( $\bar{J}_2 = 1.382 \pm 0.195 \text{ s}^{-1}$ ) nor the growth rates ( $\bar{GR}_{1.3-20 \text{ nm}} = 6.20 \pm 0.12 \text{ nm h}^{-1}$ ) differ from one site to the other on average. However, we found that, on 437 sampling days in common to the two sites, the nucleation frequency was higher at the puy de Dôme station (35.9%, 157 days) than at the low elevation station of Opme (20.8%, 91 days). The role of sulfuric acid in the nucleation process was investigated at the altitude station and no correlation was found between nucleation events and the estimated sulfuric acid concentrations. Nevertheless, the contribution of ion-induced nucleation was found to be relatively high ( $12.49 \pm 2.03\%$  of the total nucleation rate). LIDAR measurements and the evolution of the potential equivalent temperature revealed that the nucleation could be triggered either (i) within the whole low tropospheric column at the same time from the planetary boundary layer to the top of the injection layer (29.2%, 47 events), (ii) above the planetary boundary layer upper limit (43.5%, 70 events), and (iii) at low altitude and then transported, conserving dynamic and properties, at high altitude (24.8%, 40 events). This is the first time that the vertical extent of nucleation can be studied over a long observational period, allowing for a rigorous statistical analysis of the occurrence of nucleation over the whole lower troposphere. This work highlights the fact that nucleation can have occur over a large vertical extent, at least the whole low tropospheric column, and also the fact that it occurs twice as frequently as actually detected in the planetary boundary layer.

## Vertical extent of nucleation events

J. Boulon et al.

Title Page

Abstract

Introduction

Conclusions

References

Tables

Figures

◀

▶

◀

▶

Back

Close

Full Screen / Esc

Printer-friendly Version

Interactive Discussion



## 1 Introduction

The formation of new ultrafine particles from the gas phase has been observed in various continental and marine locations (see for a review Kulmala et al., 2004) indicating that nucleation followed by new particle formation (NPF) events is an ubiquitous phenomenon in the planetary boundary layer (PBL). Up to which altitude these NPF events take place, and where they are initiated is still under debate. Crumeyrolle et al. (2010) observed during airborne measurements that NPF events was limited to the PBL vertical extent while Mirme et al. (2010) have shown that sub-3 nanometers particle (nucleation tracers) could be observed throughout the tropospheric column up to the tropopause suggesting that nucleation could also occur above the PBL. Several studies show that atmospheric dynamics such as turbulence or boundary layer mixing could trigger the nucleation process (i.e. Nilsson and Kulmala, 1998; Nilsson et al., 2001). During the intensive field campaign SATURN, Stratmann et al. (2003) showed that nucleation could take place inside the residual layer and that it could be induced by the break-up of the nocturnal inversion. Furthermore, they explained the ultrafine particle concentration at a ground-based measurement site as a result of the mixing down of the freshly formed particles within the residual layer. A recent intensive field campaign using LIDAR soundings coupled with 12 helicopter particle measurements confirm that the new particle formation process is enhanced in layers of high turbulent mixing such as the residual layer (Wehner et al., 2010). Wehner and co workers also show that the NPF reported to occur in the residual layer are connected to peaks of ultrafine particle number concentrations at the ground level (Cabaw, Netherlands). Those previous studies are based on few cases (less than twenty) and most of them use particle measurement devices that allow measurement down to 3 nm. Here, we propose the first long term study of the vertical extent of the new particle formation process based on a nearly 4-yr measurement period at two different altitudes: The puy de Dôme station (1465 m a.s.l.) and the Opme station (660 m a.s.l.). Both sites were equipped with instruments which allow ions and neutral particle detection from 0.5 nm

### Vertical extent of nucleation events

J. Boulon et al.

Title Page

Abstract

Introduction

Conclusions

References

Tables

Figures

◀

▶

◀

▶

Back

Close

Full Screen / Esc

Printer-friendly Version

Interactive Discussion



to 42 nm. Hence, it allows the tracking of in situ nucleation versus transport from one site to the other. In addition to particle measurement devices, the atmospheric vertical structure and the boundary layer evolution was investigated using LIDAR measurements that were operated at about 11 km of each measurement sites.

## 2 Measurement sites

Measurements were conducted at two nearly located mid-altitude sites: the puy de Dôme station (mountain site) and Opme station (rural site). The puy de Dôme research station is located at 1465 m a.s.l. in central France (45°46' N, 2°57' E). The station is surrounded mainly by a protected area where fields and forests are predominant, the city of Clermont-Ferrand (300 000 inhabitants) being located 16 km East of the station. Meteorological parameters, including the wind speed and direction, temperature, pressure, relative humidity and radiation (global, UV and diffuse), atmospheric trace gases (O<sub>3</sub>, NO<sub>x</sub>, SO<sub>2</sub>, CO<sub>2</sub>) and particulate black carbon (BC) are monitored continuously throughout the year. Winter temperatures vary typically from -10 to +10 °C. Westerly and northerly winds are dominant. During the November–April period, the road access to the station is restricted to experimental work preventing from local contamination. The Opme station is located around 12 km South-East of the puy de Dôme station (45°42' N, 3°05' E, 660 m a.s.l.) in a rural area dominated by agricultural fields and forest. The two sites are not separated by topographical barrier so that air parcels can move free of constraint between the two sites (Fig. 1).

## 3 Instrumentation

### 3.1 Particle measurement devices

Because the puy de Dôme station is more than 50% of the time in-cloud, the aerosol sampling is performed through a whole air inlet (WAI) which ensures efficient sampling

## Vertical extent of nucleation events

J. Boulon et al.

Title Page

Abstract

Introduction

Conclusions

References

Tables

Figures

◀

▶

◀

▶

Back

Close

Full Screen / Esc

Printer-friendly Version

Interactive Discussion



**Vertical extent of nucleation events**

J. Boulon et al.

Title Page

Abstract

Introduction

Conclusions

References

Tables

Figures

◀

▶

◀

▶

Back

Close

Full Screen / Esc

Printer-friendly Version

Interactive Discussion



of both cloud droplets and interstitial aerosol in the presence of clouds. The WAI samples air at 12 m above the ground through a heated inlet that avoids ice formation. Wind velocity around the inlet head is lowered by a wind-shield to ensure efficient sampling even at elevated wind speeds. Air is sucked into a 12-cm-diameter PVC tube at a flow rate of  $30 \text{ m}^3 \text{ h}^{-1}$  subsequently sub-sampled inside the PVC tube with a 5-cm-diameter stainless-steel tube ensuring iso-kinetic sub-sampling. The stainless-steel section of the inlet is equipped with a heated section to evaporate cloud droplets and to maintain the relative humidity of sampled air at about 50%. Interstitial aerosols and evaporated cloud residues are sampled simultaneously at a constant relative humidity and can be compared in size regardless of the environmental conditions. Temperature never exceeded  $25^\circ \text{C}$  to limit aerosol volatilization. A SMPS (Scanning Mobility Particle Sizer), measured the particle number size distribution (10–400 nm) at the top of the puy de Dôme station through the WAI continuously since May 2005, with a two-minute resolution. The SMPS is composed of a condensation particle counter TSI 3010 and a Differential Mobility Analyser (DMA) columns TSI-3081. The instrument data evaluation and the seasonal variation of the aerosol size distribution are described in details in Venzac et al. (2009).

A separate short inlet was used for the AIS and NAIS sampling, directly through the station front facade, in order to avoid the re-combination of ions in the sampling line. The upper size-cut of large ions sampled through the AIS inlet is  $10 \mu\text{m}$  for a wind speed of  $2 \text{ m s}^{-1}$  and  $2 \mu\text{m}$  for; a wind speed of  $5 \text{ m s}^{-1}$  wind speed. As a result, few droplets should enter the inlet, except at wind speeds smaller than  $5 \text{ m s}^{-1}$  which is rare at the station. The mobility distributions of atmospheric positive and negative ions are measured with the AIS (Airel Ltd., Mirme et al., 2007), providing the ion size distribution in the diameter range 0.5–44 nm (mobility range:  $3.162\text{--}0.0013 \text{ cm}^2 \text{ V}^{-1} \text{ s}^{-1}$ ). The AIS sampling principle is based on the simultaneous selection of 21 different sizes of atmospheric ions of each polarity (negative and positive) along two differential mobility analyzers and their subsequent simultaneous detection using electrometers in parallel. The sample flow rate of the AIS is  $60 \text{ m s}^{-1}$ .

**Vertical extent of nucleation events**

J. Boulon et al.

[Title Page](#)[Abstract](#)[Introduction](#)[Conclusions](#)[References](#)[Tables](#)[Figures](#)[◀](#)[▶](#)[◀](#)[▶](#)[Back](#)[Close](#)[Full Screen / Esc](#)[Printer-friendly Version](#)[Interactive Discussion](#)

The AIS sampling alternated with NAIS (Neutral clusters and Air Ion Spectrometer) sampling. The NAIS is similar to the AIS, with an additional possibility to measure total particles (neutral and charged particles). However, below 2 nm, neutral particles measurement are not relevant since the post-filtering process cuts also the sampled newly formed particles (Asmi et al., 2009).

The data discussed in this paper are based on samplings achieved during more than three years from February 2007 to June 2010 for puy de Dôme site and from October 2008 up to June 2010 for Opme site. Within this period, 952 days are available for the puy de Dôme station and 437 days for Opme station.

**3.2 LIDAR measurements**

In addition to in-situ measurements and in order to characterize the atmospheric layers structure, LIDAR measurements were performed from the roof of the Laboratoire de Météorologie Physique (LaMP) (45°45' N, 3°6' E, 410 m a.s.l.). The LIDAR used in this study is a Raymetrics Rayleigh-Mie LIDAR emitting at 355 nm, with parallel and perpendicular polarization channels. The instrument provides profiles of volume backscatter and extinction coefficients of aerosol particles, the depolarisation ratio, and water-vapor-to-dry-air mixing ratio. The LIDAR returns signals strongly dependent on height  $z$  (in the case of a ground-based, vertically pointing lidar) and decreasing with  $z^2$ . Correcting the signal with  $z^2$  thus removes the height dependence.

It is well known that aerosol particles are more numerous within the PBL than in the FT, so we assume that the summit of the PBL is characterized by a modification of the light diffusion regime. Hence, the height of the planetary boundary layer is estimated by the inflexion point between the back-scattering signal dominated by Rayleigh diffusion and the back-scattering signal dominated by the Mie diffusion (strongly linked to the decrease of the particle concentration in this part of the atmosphere). An example is presented in Fig. 2. The position of the inflexion point is determined using fitting two different parts of the profile, assuming that the PBL upper boundary is located at the slope rupture point. We also estimate the height

## Vertical extent of nucleation events

J. Boulon et al.

Title Page

Abstract

Introduction

Conclusions

References

Tables

Figures

◀

▶

◀

▶

Back

Close

Full Screen / Esc

Printer-friendly Version

Interactive Discussion



of the injection layer, i.e. the interface between the PBL and the FT, using the divergence between the fit of the Rayleigh regime and the measurements assuming that its width is the height where  $\text{abs}(\text{Fit}_{\text{value}} - \text{Measurement}) > (\text{mean}(\text{Measurements}) - \text{std}(\text{Measurement}))$ . This method was compared to the WCT algorithm proposed by Brooks (2003), initially developed for marine boundary layer height retrievals. The calculated PBL height was found to be 20.7% higher on average when it was computed using our method. This difference comes from the fact that the WCT method try to find the upper limit of the main aerosol layer (i.e. the start of the decrease of the Mie regime) whereas our method was build to find the transition from Mie diffusion regime to Rayleigh diffusion regime i.e. the transition from planetary boundary layer influenced layers to free tropospheric influenced layers. Compared to WCT, this procedure seems to be better adapted to the calculation of the PBL height in mountainous area such as puy de Dôme.

## 4 Results

### 4.1 Nucleation events at the puy de Dôme station

The classification of event days was performed visually using the daily contour plot of the ion size distribution evolution. Data were first categorized into three main classes: undefined, non-event and nucleation event days. Since different types of nucleation event can be observed, event days were classified into different classes (Ia, Ib, II and Bump) according to their quality and their applicability to a growth rate analysis (Hir-sikko et al., 2005):

- Ia: Continuous growth of clusters (0.5 nm) to large particle ( $\geq 20$  nm).
- Ib: These events are not as strong as class Ia events and sometimes cluster or intermediate growth are not clearly visible on the size distribution but the growth rate calculation remains possible.

- II: A clear event is identified but the growth from clusters to large particle is not regular and the shape of the size distribution is unclear. Further analysis of the new particle formation characteristics are complex.
- Bump: A burst of clusters is detected but it is not followed by a significant growth and particle formation. Different explanations are possible such as the total consumption of the condensing vapors or a change in the air mass.

Based on the long term continuous measurements, the seasonal variation of nucleation events at the puy de Dôme station are presented in Fig. 3. Nucleation occurs around one third of the time at the puy de Dôme station (30.8%) which is in agreement with the previous study made by Venzac et al. (2007). Unfortunately, due to many discontinuities of the measurements, we cannot perform such an analysis for Opme. The observed seasonal variation (Fig. 3) is not very pronounced but we can distinguish two maxima (one during early spring and the other one during the early autumn). At other sites where nucleation events show a seasonal variation the maximal occurrence was usually observed during the spring and autumn seasons as well (Manninen et al., 2010) except for the Mt. Everest station (Venzac et al., 2008) where the maximal occurrence of nucleation events is during the summer. At Mt. Everest, authors explain this phenomenon as a result of the strong upslope wind that occurs during daytime in the summer and brings condensable vapours to the measurement site. The minimal occurrence frequency is always observed during winter months partly due to a lower photochemical activity (Venzac et al., 2008; Manninen et al., 2010; Boulon et al., 2010).

Different steps can describe the NPF process. We chose 4 different boundary diameters (1.3, 3, 7 and 20 nm) as representative of different growth steps and to compute growth rates between 1.3–3, 3–7 and 7–20 nm for Ia and Ib classes of event. A more detailed description of the growth rate calculation procedure can be found in Boulon et al. (2010). Average growth rates in each size class are respectively  $3.22 \pm 0.25$ ,  $6.52 \pm 0.20$  and  $8.85 \pm 0.14 \text{ nm h}^{-1}$ , and the mean GR for the entire nucleation mode (1.3–20 nm) is  $6.20 \pm 0.12 \text{ nm h}^{-1}$ . The GR depends on (i) the chemical nature of the

**Vertical extent of nucleation events**

J. Boulon et al.

Title Page

Abstract

Introduction

Conclusions

References

Tables

Figures

◀

▶

◀

▶

Back

Close

Full Screen / Esc

Printer-friendly Version

Interactive Discussion



## Vertical extent of nucleation events

J. Boulon et al.

Title Page

Abstract

Introduction

Conclusions

References

Tables

Figures

◀

▶

◀

▶

Back

Close

Full Screen / Esc

Printer-friendly Version

Interactive Discussion



clusters and of the condensable vapours (ii) the particle sizes. For a given constant condensable vapour concentration, the condensational dynamic equation (Dal Maso et al., 2002) predicts that the GR is decreasing with increasing particle diameters. The larger GR observed for larger particle diameters indicate that either condensing vapours concentrations increase with time, in parallel to the particle growth or/and the nature of condensing species evolves towards lower volatility compounds during the oxidation process as show by Aumont et al. (2005). Computed GRs from the puy de Dôme data are comparable to GRs computed for other mountain sites (i.e. Shaw, 2007; Nishita et al., 2008; Venzac et al., 2008; Boulon et al., 2010) even though those latter present a wide range of variation because of particular local environment (i.e. vegetation, pollution). Formation rates for charged ( $J_2^\pm$ ) and neutral ( $J_2$ ) aerosols were computed according to Eqs. (1 and 2) (from Kulmala et al., 2007):

$$J_2 = \frac{dN_{2-3}}{dt} + \text{CoagS}_2 \times N_{2-3} + \frac{f}{1\text{nm}} \text{GR}_{1.3-3} N_{2-3} \quad (1)$$

$$J_2^\pm = \frac{dN_{2-3}^\pm}{dt} + \text{CoagS}_2 \times N_{2-3}^\pm + \frac{f}{1\text{nm}} \text{GR}_{1.3-3} N_{2-3}^\pm + \alpha \times N_{2-3}^\pm N_{<3}^\mp - \beta \times N_{2-3} N_{<2}^\pm \quad (2)$$

where  $N_{2-3}^\pm$  is the ion number concentration (positive or negative ions) ( $\#\text{cm}^{-3}$ ) in diameter range from 2 to 3 nm and  $N_{<x}^\pm$  is the ion number concentration below  $x$  nm.  $\text{CoagS}_2$  is the coagulation sink of 2 nm particles ( $\text{s}^{-1}$ ).  $\alpha$  and  $\beta$  are respectively the ion-ion recombination coefficient and the ion-neutral attachment coefficient and were assumed to be equal respectively to  $1.6 \times 10^{-6} \text{cm}^3 \text{s}^{-1}$  and  $1 \times 10^{-8} \text{cm}^3 \text{s}^{-1}$  (Tammet and Kulmala, 2005). The factor  $f$  represents the fraction of the ion population in a size range from 2 to 3 nm which are activated for the growth. In this study we assumed this factor to be equal to unity. The time derivative of  $N_{2-3}$  is directly obtained from the NAIS measurements.  $\text{CoagS}_2$  is derived from NAIS data. The mean formation

rate of charged and neutral particles are  $0.071 \pm 0.087$  respectively for positive ions,  $0.0747 \pm 0.0788$  for negative ions, and  $1.382 \pm 0.195$  for neutral species. From those results, the ion-induced nucleation (IIN) rate was computed and the mean contribution of ion to the total formation rate was found to be  $12.49 \pm 2.03\%$ . At other continental high elevation sites, a high IIN contribution to the nucleation process was also pointed out: 21.8% for the Jungfraujoch high altitude station (3580 m a.s.l., Switzerland, Boulon et al., 2010) and 5% for Hohenpeissenberg (980 m a.s.l, Germany, Manninen et al., 2010) in comparison to boundary layer sites (Manninen et al., 2010 and Iida et al., 2006, 2.6% in average on both study). These results suggest that IIN is favoured at high elevations.

#### 4.1.1 The role of sulfuric acid

Sulfuric acid concentrations were estimated using a parametrization from Petäjä et al. (2008). Hence  $\text{H}_2\text{SO}_4$  real concentrations could be different from our calculations, but their time variations should be respected. The difference in sulfuric acid concentrations calculated during nucleation event days and non-event days was tested with the Welch's t-test (t-test for two samples with unequal variance and unequal population). We found that the null hypothesis of identical average scores could not be rejected at the threshold of 5% (i.e. sulfuric acid concentrations are not statistically different between event and non-event days). Furthermore, no linear correlation was found between sulfuric acid concentrations averages (calculated over the 09:00–11:00 time period) and the particle formation rate  $J$  ( $r = -0.4365$ ). This result is in agreement with the analysis of the nucleation events occurring at the Jungfraujoch station (Boulon et al., 2010). It is likely that, at the puy de Dôme station and at the Jungfraujoch station, condensing compounds other than  $\text{H}_2\text{SO}_4$ , such as volatile organic compounds, must be involved in the new particle formation process. This assumption was also pointed out by from chamber experiments (Metzger et al., 2010). In order to test this hypothesis, we also tested different nucleation parametrizations involving sulfuric acid (Table 1, #1) and we found that the formation rate parametrizations do not correlate

### Vertical extent of nucleation events

J. Boulon et al.

Title Page

Abstract

Introduction

Conclusions

References

Tables

Figures

◀

▶

◀

▶

Back

Close

Full Screen / Esc

Printer-friendly Version

Interactive Discussion



with the observed  $J$ . Other parametrizations of charged formation rate involving a preexisting cluster number concentrations and (i) sulfuric acid (Table 1, #3 and 5) or (ii) the global radiation as a proxy of photochemically induced nucleation (Table 1, #2 and 4) were also tested. It appears that  $J_{2\pm}$  models involving global radiations slightly correlate with observed  $J_{2\pm}$ . On the contrary, parametrizations that use sulfuric acid concentrations could not explain the observed charged formation rates. Those results corroborate the hypothesis that photochemical processes involving other compounds than  $\text{H}_2\text{SO}_4$ , such as organic vapour, are more relevant to describe particle formation rate at the puy de Dôme station.

#### 4.1.2 Air mass backtrajectories influence

We investigated the impact of the air mass origin on the occurrence of a nucleation event using the three days air mass back trajectories computed with the HYSPLIT transport and dispersion model (Draxler and Rolph, 2003). Air masses were classified according to their geographical origin with a resolution of  $10^\circ \times 10^\circ$ . Since this model uses as input data meteorological variables with  $10^\circ$  of resolution, it cannot describe local air mass motion such as topographical effects or local convection. Assuming that simulated altitude outputs are overestimated for high altitude sites, they will not be discussed in this paper. Five different classes were created depending of the air mass' origin: atlantic, african, polar, eastern and western european air masses (the detailed classification can be found in Boulon et al., 2010). Tunved et al. (2005) estimated the aerosol turnover time of Aitken particles to be in the range of 1–2 days, while accumulation mode turnover time was estimated to be in the order of 2–3 days. Hence, we chose to compute three-day backtrajectories. Since the air mass origin and path to the measurement site do not differ significantly between 00:00 and 12:00, only results for 12:00 will be included in our analysis (Fig. 4). The calculation was done over all both sites common observed days, 437 days. Air mass back-trajectories and origins are respectively reported in Fig. 4 and Table 2.

## Vertical extent of nucleation events

J. Boulon et al.

[Title Page](#)[Abstract](#)[Introduction](#)[Conclusions](#)[References](#)[Tables](#)[Figures](#)[◀](#)[▶](#)[◀](#)[▶](#)[Back](#)[Close](#)[Full Screen / Esc](#)[Printer-friendly Version](#)[Interactive Discussion](#)

The station is mainly under the influence of western air masses (i.e. from atlantic and continental western europe areas, Fig. 4). They represent 87.3% of air masses reaching the sampling site and are associated to 88.8% of the nucleation events. Air masses from africa and eastern europe represent 10.5% of total air masses and 7.5% of the total nucleation events. Polar air masses are very rare (2.2% of the total air masses and 3.7% of the observed nucleation) but have the highest nucleating ratio (Table 2). Those results suggest that there is no link between nucleation events and air mass origin since nucleating ratios of all air masses are not significantly different. It can be seen that non-nucleating air masses originate from farther west suggesting they travel at high wind speed at higher altitude, and hence they are less influenced by fresh boundary layer inputs. The seasonality of air mass types reaching the PdD station was studied by Venzac et al. (2008) who showed that western air masses reaching the puy de Dôme have travelled over longer distances during winter compared to summer. Hence another explanation for lower nucleation frequencies in more distant western air masses is because they coincide with winter conditions.

## 5 Comparison of nucleation events between the two sites

We investigated the cases when nucleation occurs (1) only at one station (puy de Dôme or Opme) and (2) at both sites. We reduced the data set to days for which data are simultaneously available for the two sites. On 437 days when data was available at both sites, nucleation occurred on 161 days (i.e. 36.8% of the time). On 161 event days, 157 events (97.5% of detected events) were detected at the puy de Dôme station and 91 (56% of detected events) at the low elevation station of Opme. Those first results show that the nucleation process is clearly enhanced at the altitude station. This first observation can be detailed with statistical data presented on Table 3. 95.6% of events (87) detected at Opme station were also detected at the puy de Dôme station whereas only 4 events are detected at the low elevation station only, indicating that the new particle process usually occurs at a large vertical extent. On the contrary,

## Vertical extent of nucleation events

J. Boulon et al.

Title Page

Abstract

Introduction

Conclusions

References

Tables

Figures

◀

▶

◀

▶

Back

Close

Full Screen / Esc

Printer-friendly Version

Interactive Discussion



considering the events detected at the elevation station of puy de Dôme, 44.5% of these events (70 events) were not detected at the lower altitude site. Based on those observations, all the nucleation events were classified into four different categories according if the event is detected (i) at the puy de Dôme station only (case “P”), (ii) at the Opme station only (case “O”), (iii) at both measurement sites and at the same time (case “D<sub>S</sub>”) or (iv) at both sites but not at the same time (case “D<sub>D</sub>”). Average contour plots of each case are presented in Fig. 5. In the following section, we present a closer look at the atmospheric composition corresponding to each case, in order to investigate the factors influencing one or the other configuration.

## 5.1 The atmospheric composition

Figure 6 shows a comparison of the different atmospheric parameters detected at the puy de Dôme station, averaged over all cases of nucleation event at the PdD station (Nuc, grey bar) or over all cases of non-event at the PdD station (Nev, grey bar). Data reported are parameters averaged over the 09:00–11:00 time period, which is assumed to correspond best to the nucleation period. Furthermore, we divided the data-set into two different sub-groups, according to cloud presence at the puy de Dôme site. This procedure allowed us to analyze the influence of various atmospheric parameters independently of the presence of clouds at the site.

Roughly, no significant differences can be outlined between event and non-event days for parameters available for this study. However, in general, parameters present a higher variability during nucleation event days, compared to non-event days. The negative effect of a strong relative humidity is clearly observed as previously shown by Venzac et al. (2007), presumably because of the strong condensational sink that cloud droplets offer to the nucleating/condensing species. We also point out that the average O<sub>3</sub> concentration is lower in case of event days compare to non-event days. The scavenging role of clouds on gases is revealed by the analysis of the B part of Fig. 6 where it can be seen that atmospheric concentrations of SO<sub>2</sub> and O<sub>3</sub> are two times lower during “in-cloud” conditions. Going into more specific cases, Fig. 6 reveals

Title Page

Abstract

Introduction

Conclusions

References

Tables

Figures

◀

▶

◀

▶

Back

Close

Full Screen / Esc

Printer-friendly Version

Interactive Discussion



that the atmospheric composition is roughly the same when a nucleation event is detected at the puy de Dôme station, no matter if the event is detected or not at the Opme station simultaneously (comparison of the grey-Nuc bar and orange bar). On the contrary, we show that the situation is very different when the nucleation occurs only at the low elevation site (Fig. 6, yellow bar). In fact, in case (O), we show that all measured parameters have the same median values as during a typical non-event day at the puy de Dôme station, i.e. higher relative humidity and higher ozone concentrations.

In a recent paper, Boulon et al. (2010) have shown that nucleation at the Jungfraujoch high altitude station could be linked to an increase of the condensational sink (CS) previous to the onset of the nucleation process, suggesting that the presence of condensing vapours probably associated to these high CS are driving the NPF events. At the puy de Dôme site, the mean CS computed before the nucleation onset (06:00–09:00 time period) and when liquid water content (LWC) is lower than  $0.02 \text{ gm}^{-3}$  (no cloud or not “in-cloud” conditions) are reported in Fig. 7. We found that, on average, the CS is lower for event days ( $3.73 \pm 0.11 \times 10^{-3} \text{ s}^{-1}$ ) than for non-event days ( $5.17 \pm 0.15 \times 10^{-3} \text{ s}^{-1}$ ) (grey bars, respectively named Nuc and Nev), illustrating the inhibiting effect of a high CS on nucleation as often found in the literature. The CS calculated when the event takes place at both stations ( $3.96 \pm 0.20 \times 10^{-3} \text{ s}^{-1}$ , orange bar) is slightly higher than when nucleation occurs only at the higher elevation one ( $3.50 \pm 0.11 \times 10^{-3} \text{ s}^{-1}$ , green bar). Again, a strong difference is observed in case of “O” type events (Fig. 7, yellow bar). In those cases, the CS is two times larger than the one observed in case of nucleation at the puy de Dôme station (Fig. 7, Nuc). Our hypothesis is that in case of “O” events, the site is in the vicinity of clouds (as will be shown later) and aerosols might still be hydrated, shifting the distribution to higher sizes and therefore increasing the condensation surface.

To summarize, at the puy de Dôme station, high condensational sinks seem to inhibit the nucleation process. This result is opposite to what Boulon et al. found at Jungfraujoch (JFJ). The JFJ is located at a higher altitude, (3580 m a.s.l.), and surrounded by areas mainly covered by snow, thus presumably a more remote site, generally poor

**Vertical extent of nucleation events**

J. Boulon et al.

Title Page

Abstract

Introduction

Conclusions

References

Tables

Figures

◀

▶

◀

▶

Back

Close

Full Screen / Esc

Printer-friendly Version

Interactive Discussion



of condensing vapours which are the limiting parameter for nucleation. The puy de Dôme station is located at a lower altitude, surrounded by a coniferous forest and can be strongly influenced by the planetary boundary layer during the day during summer (Venzac et al., 2008). The presence of condensing vapours is less a limiting factor for the occurrence of nucleation. The CS, however, is calculated at the puy de Dôme station to be one order of magnitude higher than the at JFJ, and it is obviously limiting the occurrence of NPF events at the site.

In the following, each category of nucleation event (O, P, D<sub>S</sub> and D<sub>D</sub>) will be studied separately. For each type of events, we will report the corresponding tropospheric structure of the atmosphere using ground based LIDAR measurements and potential equivalent temperature,  $\theta_e$ , calculation according to the Bolton procedure (Bolton, 1980). Over the measurement period, LIDAR data are available for 132 days. When no LIDAR data are available, two air masses or atmospheric layers will be considered the same if (i) the two  $\theta_e$  temporal evolutions are strongly correlated with each other during the nucleation process, and, (ii) the two equivalent potential temperatures are the same within the uncertainties of measurements. Uncertainties were computed using the classical error propagation theory, it was estimate at  $\pm 4.7$  K for  $\sigma = 1$ , i.e.  $\Delta\theta_e \leq 4.7$  K.

## 5.2 O cases: nucleation events at the Opme station only

Nucleation events that occur only at the Opme station are very rare: only 4 events occurred on 437 observed days (4.4% of the total observed nucleation events detected at Opme). Unfortunately, no LIDAR data are available for those events. As mentioned above, those cases present all characteristics in term of atmospheric chemical properties of a non-event day for the puy de Dôme station: high relative humidity associated with a high CS. Going further in the analysis revealed that in each O case, when the nucleation is triggered at Opme station, clouds are detected at the puy de Dôme station (Fig. 5, case O) and likely interrupted the nucleation process through the scavenging of condensable vapours and/or pre-existing clusters by cloud droplets (Venzac et al., 2007).

## Vertical extent of nucleation events

J. Boulon et al.

[Title Page](#)[Abstract](#)[Introduction](#)[Conclusions](#)[References](#)[Tables](#)[Figures](#)[◀](#)[▶](#)[◀](#)[▶](#)[Back](#)[Close](#)[Full Screen / Esc](#)[Printer-friendly Version](#)[Interactive Discussion](#)

**Vertical extent of nucleation events**

J. Boulon et al.

Title Page

Abstract

Introduction

Conclusions

References

Tables

Figures

◀

▶

◀

▶

Back

Close

Full Screen / Esc

Printer-friendly Version

Interactive Discussion



In the following, we analyze an example but it is representative of all four “O” cases. Also in term of boundary layer dynamics, the same pattern is always observed. As for the 12 August 2007, the two sites always seem to be located within the planetary boundary layer when the nucleation is onset. This assertion is based on the comparison between the temporal evolution of the equivalent potential temperature ( $\theta_e$ ) at puy de Dôme and Opme. Figure 8 shows the temporal evolution of  $\theta_e$  and the correlation of this thermodynamic tracer between the two sites at three different periods of the day (00:00 to 07:00, 07:00 to 16:00 and 16:00 to 00:00) and during the nucleation period (between 09:00 and 11:00). During the night and early morning, the two sites have the same  $\theta_e$  but the low correlation ( $r(\theta_e) = 0.4930$ ) indicates that the two sites are in different atmospheric layers. After 07:00 and until around 09:30, the two equivalent potential temperatures become equal and their evolution is strongly correlated ( $r(\theta_e) = 0.8391$ ). After 09:30, the  $\theta_e(\text{PdD}) > \theta_e(\text{Opme})$  but their evolution is still strongly correlated ( $r_{9:30-16:00} = 0.9545$ ). This could indicate that the two sites are not in the same atmospheric layer but in two different layers which are connected or in the same unhomogeneous layer.

During the morning, the PdD station is in “in-cloud” condition between 07:00 and 09:30, mean values of the relative humidity (RH) and liquid water content (LWC) are respectively 100% and  $0.089 \text{ g m}^{-3}$ , when the nucleation is triggered at Opme site. Later during the day, the PdD station is still in “in-cloud” condition or in the vicinity of clouds (RH and LWC between 07:00 and 16:00 are respectively 96.0% and  $0.024 \text{ g m}^{-3}$  in average). This type of event do not inform us on the spatial extent of the nucleation but two hypothesis could be formulated: (i) the spatial extent of the nucleation is very low and it occurs only within a small geographical area before all reactive and condensable species has been completely consumed, (ii) the nucleation could occur within the whole column in the PBL but condensable vapors have been scavenged by cloud droplets at the altitude site. According to statistical analysis of the events repartition between the two sites, it's likely that the second hypothesis is the most probable. As we will show in the following, when the nucleation is triggered at Opme site, the phenomenon could

also be detected at the altitude station (87 events on 91 measured at Opme station).

In the following, we investigate deeper the spatial extent of the nucleation through the study of what happen when the nucleation occur at the altitude site (cases “P”, “D<sub>S</sub>” and “D<sub>D</sub>”).

### 5.3 P cases: nucleation events at the puy de Dôme station only

This case represents 43.5% of the total number of nucleation events observed in this study (70 events on the 161 events, Table 3). Among these nucleation events, LIDAR data are available for 10 days.

The average daily time series of the cluster and particle size distributions at both sites is shown in Fig. 5, case “P”. As seen, no nucleation event is detected at the Opme site, the two peaks of particle concentration seen at Opme station on early morning and at the end of the afternoon are due to traffic-related emissions. In Fig. 9 the temporal evolution of the equivalent potential temperature at both sites,  $\theta_e$ , is reported for a typical “P” case event (13 March 2009). All “P” case event days show the same pattern.

The diurnal evolution of  $\theta_e$ , which is lower at the altitude site at night and early morning (unstable conditions), suddenly increased until reaching the same value as at the low elevation site, within uncertainties. This clearly indicates a change in atmospheric physical properties.

The evolution of  $\theta_e$  between the two sites associated with a non-equality between the equivalent potential temperatures highlights that air parcels of each site are very weakly connected with each other during the nucleation process (in the case of 13 March 2009,  $r(\theta_e) = 0.3080$  and  $\Delta\theta_e = -7.2532$  K). This hypothesis is confirmed by the LIDAR measurements. The  $z^2$  LIDAR back-scattering signal (we will name it the  $z^2$ -signal in the following), reported Fig. 10 (left panel) is consistent with this interpretation and clearly shows that the two sites are located within different atmospheric layers. A more precise analysis of the  $z^2$ -signal was performed and is reported on the right panel of the Fig. 10. It confirms that the two sites are located in two different atmospheric layers: Opme site is located within the PBL while the PdD is located at the interface between

## Vertical extent of nucleation events

J. Boulon et al.

Title Page

Abstract

Introduction

Conclusions

References

Tables

Figures

◀

▶

◀

▶

Back

Close

Full Screen / Esc

Printer-friendly Version

Interactive Discussion



the PBL and the FT, and more precisely above the upper boundary in what we defined as the injection layer. The average height of the PBL computed using our procedure between 09:00 and 11:00 for “P” cases is  $1218 \pm 187$  m a.s.l., hence confirming that the puy de Dôme station is not located in the same layer than Opme during the nucleation process. By the end of the afternoon the LIDAR signal shows a subsidence of atmospheric layers when the thermic convection stops, leading to an atmospheric disconnection between the two sites. This is illustrated by an increasing of  $\Delta\theta_e$  between the two sites and a decrease of the  $\theta_e$  pearson correlation between the two stations.

#### 5.4 $D_x$ cases: nucleation events at both sites

In opposition to what happen in the cases (P), in D cases the nucleation process occurs at the two measurement sites. This case represents 54% of the total number of nucleation events observed in this study (87 events on the 161 observed events, Table 3). Among these nucleation events, LIDAR data are available for 26 days. Two different sub-cases could be pointed out: (i) the two sites are located within the same atmospheric layer when the nucleation is triggered (47 events), and, (ii) the nucleation is triggered at one site and then through atmospheric mixing, the nucleating air parcel is transported to the other site (40 events).

##### 5.4.1 Simultaneous events ( $D_S$ )

This phenomenon is observed on 47 days i.e. one third of the total nucleation events observed at the puy de Dôme station and 54% of the “both sites events”. As seen on the temporal evolution of the aerosol numer-size distribution (Fig. 5, case  $D_S$ ), the two events detected at both measurement sites start at the same time and present similar shapes and characteristics. In opposition to what we observed on the previous cases, here the evolution  $\theta_e$  is well correlated along the day (Fig. 11) and especially during the nucleation process where the median Pearson’s correlation is 0.739 for all  $D_S$  events.

Title Page

Abstract

Introduction

Conclusions

References

Tables

Figures

◀

▶

◀

▶

Back

Close

Full Screen / Esc

Printer-friendly Version

Interactive Discussion



**Vertical extent of nucleation events**

J. Boulon et al.

[Title Page](#)[Abstract](#)[Introduction](#)[Conclusions](#)[References](#)[Tables](#)[Figures](#)[◀](#)[▶](#)[◀](#)[▶](#)[Back](#)[Close](#)[Full Screen / Esc](#)[Printer-friendly Version](#)[Interactive Discussion](#)

The LIDAR signal analysis (Fig. 12) confirms what is deduced from the analysis of the temporal evolution of  $\theta_e$ . As seen in Fig. 12, the two sites are not exactly located in the same atmospheric layer. However, and contrarily to what is observed on “P” cases, the two sites are strongly connected: the puy de Dôme station is located inside the injection layer while Opme station is within the lower boundary layer.

In this case of simultaneous nucleation, we can conclude that nucleation occurs at the same time within the whole planetary boundary layer column. This means that all the elements required to trigger nucleation are homogeneously distributed within the PBL.

#### 5.4.2 Non simultaneous nucleation ( $D_D$ )

In “ $D_D$ ” cases (40 events), the nucleation process occurs at both sites but it do not start at the same time at both stations. However, as seen on temporal evolution of aerosols distribution (Fig. 5, case  $D_D$ ) the nucleation events present very similar shape and characteristics at both site. This observation suggests that the two events are connected. An example of the evolution of theta is given in Fig. 13. All “ $D_D$ ” cases show the same theta evolution pattern. The non-correlated evolution of  $\theta_e$  (Fig. 13) shows that the two sites seem to be located within two independent atmospheric layers when the nucleation is triggered at the low elevation station ( $r(\theta_e) = -0.1370$  and  $\Delta\theta_e = -7.118 \pm 1.093$  K). The median correlation of the equivalent potential temperature during the nucleation event for all  $D_D$  events is 0.586. This value is lower compared to the one observed for  $D_S$  cases indicating that the atmospheric connection between the two sites is weaker.

On the contrary, LIDAR measurements (Fig. 14) indicate that the two measurement sites are located within the planetary boundary layer (the limit, in the case of 21 May 2009, was found to be  $1703 \pm 515$  m a.s.l.). The time delay of the nucleation at the altitude site could be due to a strong stratification of the boundary layer.

For all “ $D_D$ ” and “ $D_S$ ” events, we computed the elevation of the top boundary of the PBL using the procedure we detailed Sect. 2.1.2. The average height is

1453 ± 520 m a.s.l. In “D<sub>x</sub>” cases, the PBL mean height is higher than in the “P” cases and it also shows a higher variability. The analysis of the potential temperature vertical gradient  $\frac{\partial\theta}{\partial z}$  indicates that in both cases (D<sub>D</sub> and D<sub>S</sub>), the atmosphere is vertically stable. This indicates that the turbulent convection is not well developed at the time of the nucleation onset. This observation confirms that, in case of the simultaneous nucleation, all components required to trigger nucleation are homogeneously distributed within the PBL whereas in the D<sub>D</sub> cases, those components might be transported through advective motion of air parcels from low altitude to the high altitude station. This hypothesis is in agreement with the  $\theta_e$  evolution at both site which present a temporal shift equal to the time delay observed on the nucleation event.

## 6 Conclusions

We investigated the occurrence of nucleation at a high elevation site, (puy de Dôme, center of France), through long term measurements of clusters and particle size distributions. We first found that the nucleation frequency is quite high (30% of observed days in average) and present a slight seasonal variation, with two maxima during early spring and autumn and a minimum during winter. From our observations, formation rates of 2 nm particles and their growth rate to larger size were computed using NAIS and AIS data. Average  $J_2$  are respectively  $\bar{J}_2 = 1.382 \pm 0.195 \text{ s}^{-1}$ , and average GR are  $\bar{GR}_{1.3-20 \text{ nm}} = 6.20 \pm 0.12 \text{ nm h}^{-1}$ . Measurements of charged and neutral particles indicate that ion induced nucleation (IIN) contributed by  $\bar{IIN} = 12.49 \pm 2.03\%$  to the total nucleation. Compared to other European low elevation sites ( $\bar{IIN} = 3.55 \pm 3.73$ ), the IIN calculated at the puy de Dôme is quite high but close to the one computed at other European altitude sites ( $\bar{IIN} = 15.10 \pm 6.96$ ) (Manninen et al., 2010; Boulon et al., 2010), suggesting that the ion contribution to nucleation is enhanced at high altitudes.

The relationship between the atmospheric composition and nucleation occurrence was analyzed and no significant difference was found between event and non-event

## Vertical extent of nucleation events

J. Boulon et al.

[Title Page](#)[Abstract](#)[Introduction](#)[Conclusions](#)[References](#)[Tables](#)[Figures](#)[◀](#)[▶](#)[◀](#)[▶](#)[Back](#)[Close](#)[Full Screen / Esc](#)[Printer-friendly Version](#)[Interactive Discussion](#)

**Vertical extent of nucleation events**

J. Boulon et al.

[Title Page](#)[Abstract](#)[Introduction](#)[Conclusions](#)[References](#)[Tables](#)[Figures](#)[◀](#)[▶](#)[◀](#)[▶](#)[Back](#)[Close](#)[Full Screen / Esc](#)[Printer-friendly Version](#)[Interactive Discussion](#)

days for most atmospheric parameters except for relative humidity, ozone concentration and condensational sink. This three parameters are all significantly lower in case of nucleation event at the puy de Dôme site. This later observation does not corroborate the results reported from the Jungfraujoch high alpin site, where authors found that new particle formation events frequency surprisingly increases with the condensational sink (Boulon et al., 2010). Different condensable vapor/CS ratio are likely very different at the two stations. Furthermore, we found that sulfuric acid do not play a key role in the nucleation process at puy de Dôme, as also shown at the Jungfraujoch station, suggesting that at those two altitude sites, the nucleation is mainly influence by other condensable vapors such as VOCs.

Combining the puy de Dôme measurements with measurements at the lower altitude station of Opme, we were able to investigate the vertical extent of the nucleation process in this rural mountainous area. We show that nucleation is a high altitude enhanced process. Nucleation is very rarely detected at the lower elevation site only (2.5%), and when it is, it is always linked to the presence of a cloud at the altitude station. On the contrary, 43.5% of observed events occur at the high altitude station only (“P” cases), above planetary boundary layer upper limit. Lidar measurements indeed indicate that during P cases, the average height of the PBL,  $1218 \pm 187$  m a.s.l. is lower than the height of the puy de Dôme station, i.e. 1465 m a.s.l.

At last, we demonstrate that the nucleation also often occurs within the whole planetary boundary layer column (54% of observed events). During those events, the PBL average height during the nucleation process was computed to be  $1453 \pm 520$  m a.s.l. which is close to the puy de Dôme station elevation confirming a high vertical extent of the boundary layer. Two sub-types of events were identified: ( $D_S$ , 29.2% of observed events), simultaneous nucleation at both sites and ( $D_D$ , 24.8% of observed events) time-shifted nucleation. During “ $D_D$ ” cases, nucleation is triggered a the low elevation site and then triggered at higher altitude.

These observations suggest that the nucleation process can have a wide vertical extent, equivalent to the PBL extent, but can also be triggered at high altitude only,

above the PBL upper limit. In a more general consideration, this work highlights that nucleation occurs twice as frequently as actually detected in the planetary boundary layer.



The publication of this article is financed by CNRS-INSU.

## References

- Asmi, E., Sipilä, M., Manninen, H. E., Vanhanen, J., Lehtipalo, K., Gagné, S., Neitola, K., Mirme, A., Mirme, S., Tamm, E., Uin, J., Komsaare, K., Attoui, M., and Kulmala, M.: Results of the first air ion spectrometer calibration and intercomparison workshop, *Atmos. Chem. Phys.*, 9, 141–154, doi:10.5194/acp-9-141-2009, 2009. 8254
- Aumont, B., Szopa, S., and Madronich, S.: Modelling the evolution of organic carbon during its gas-phase tropospheric oxidation: development of an explicit model based on a self generating approach, *Atmos. Chem. Phys.*, 5, 2497–2517, doi:10.5194/acp-5-2497-2005, 2005. 8257
- Bolton, D.: The Computation of Equivalent Potential Temperature, *Mon. Weather Rev.*, 108, 1046–1053, 1980. 8263
- Boulon, J., Sellegri, K., Venzac, H., Picard, D., Weingartner, E., Wehrle, G., Collaud Coen, M., Büttikofer, R., Flückiger, E., Baltensperger, U., and Laj, P.: New particle formation and ultrafine charged aerosol climatology at a high altitude site in the Alps (Jungfraujoch, 3580 m a.s.l., Switzerland), *Atmos. Chem. Phys.*, 10, 9333–9349, doi:10.5194/acp-10-9333-2010, 2010. 8256, 8257, 8258, 8259, 8262, 8268, 8269
- Brooks, I. M.: Finding Boundary Layer Top: Application of a Wavelet Covariance Transform to Lidar Backscatter profiles, *J. Atmos. Ocean. Technol.*, 20, 1092–1105, 2003. 8255

ACPD

11, 8249–8290, 2011

## Vertical extent of nucleation events

J. Boulon et al.

Title Page

Abstract

Introduction

Conclusions

References

Tables

Figures

◀

▶

◀

▶

Back

Close

Full Screen / Esc

Printer-friendly Version

Interactive Discussion



**Vertical extent of nucleation events**

J. Boulon et al.

Title Page

Abstract

Introduction

Conclusions

References

Tables

Figures

◀

▶

◀

▶

Back

Close

Full Screen / Esc

Printer-friendly Version

Interactive Discussion



- Crumeyrolle, S., Manninen, H. E., Sellegrì, K., Roberts, G., Gomes, L., Kulmala, M., Weigel, R., Laj, P., and Schwarzenboeck, A.: New particle formation events measured on board the ATR-42 aircraft during the EUCAARI campaign, *Atmos. Chem. Phys.*, 10, 6721–6735, doi:10.5194/acp-10-6721-2010, 2010. 8251
- 5 Dal Maso, M., Kulmala, M., Lehtinen, K. E. J., Mäkelä, J., Aalto, P., and O'Dowd, C.: Condensation and coagulation sinks and formation of nucleation mode particles in coastal and boreal forest boundary layer, *J. Geophys. Res.*, 107(D19), 8097, doi:doi:10.1029/2001JD001053, 2002. 8257
- Draxler, R. R. and Rolph, G. D.: HYSPLIT (Hybrid Single-Particle Lagrangian Integrated Trajectory) Model access via NOAA ARL READY website (<http://www.arl.noaa.gov/ready/hysplit4.html>), NOAA Air Resources Laboratory, Silver Spring, MD, 2003. 8259
- 10 Hirsikko, A., Laakso, L., Hörrak, U., Aalto, P., Kerminen, V.-M., and Kulmala, M.: Annual and size dependant variation of growth rates and ion concentrations in boreal forest, *Bor. Env. Res.*, 10, 2005. 8255
- 15 Iida, K., Stolzenburg, M., McMurry, P., Dunn, M. J., Smith, J. N., Eisele, F., and Keady, P.: Contribution of ion-induced nucleation to new particle formation: Methodology and its application to atmospheric observations in Boulder, Colorado, *J. Geophys. Res.*, 111, D23201, doi:10.1029/2006JD007167, 2006. 8258
- Kerminen, V.-M., Petäjä, T., Manninen, H. E., Paasonen, P., Nieminen, T., Sipilä, M., Junninen, H., Ehn, M., Gagné, S., Laakso, L., Riipinen, I., Vehkamäki, H., Kurten, T., Ortega, I. K., Dal Maso, M., Brus, D., Hyvärinen, A., Lihavainen, H., Leppä, J., Lehtinen, K. E. J., Mirme, A., Mirme, S., Hörrak, U., Berndt, T., Stratmann, F., Birmili, W., Wiedensohler, A., Metzger, A., Dommen, J., Baltensperger, U., Kiendler-Scharr, A., Mentel, T. F., Wildt, J., Winkler, P. M., Wagner, P. E., Petzold, A., Minikin, A., Plass-Dülmer, C., Pöschl, U., Laaksonen, A., and Kulmala, M.: Atmospheric nucleation: highlights of the EUCAARI project and future directions, *Atmos. Chem. Phys.*, 10, 10829–10848, doi:10.5194/acp-10-10829-2010, 2010. 8274
- 20 Kulmala, M., Vehkamäki, H., Petäjä, T., Dal Maso, M., Lauri, A., Kerminen, V.-M., Birmili, W., and McMurry, P.: Formation and growth rates of ultrafine atmospheric particles: a review of observations, *J. Aerosol Sci.*, 35, 143–176, 2004. 8251
- 25 Kulmala, M., Riipinen, I., Sipilä, M., Manninen, H. E., Petäjä, T., Junninen, H., Dal Maso, M., Mordas, G., Mirme, A., Vana, M., Hirsikko, A., Laakso, L., Harrison, R., Hanson, I., Leung, C., Lehtinen, K. E. J., and Kerminen, V.-M.: Towards direct measurements of atmospheric

**Vertical extent of nucleation events**

J. Boulon et al.

[Title Page](#)[Abstract](#)[Introduction](#)[Conclusions](#)[References](#)[Tables](#)[Figures](#)[◀](#)[▶](#)[◀](#)[▶](#)[Back](#)[Close](#)[Full Screen / Esc](#)[Printer-friendly Version](#)[Interactive Discussion](#)

nucleation, *Science*, 318a, 89–92, 2007. 8257

Manninen, H. E., Nieminen, T., Asmi, E., Gagné, S., Häkkinen, S., Lehtipalo, K., Aalto, P., Kivekäs, N., Vana, M., Mirme, A., Mirme, S., Hörrak, U., Plass-Dülmer, C., Stange, G., Kiss, G., Hoffer, A., Moerman, M., Henzing, B., Brinkenberg, M., Kouvarakis, G. N., Bougiatioti, K., O'Dowd, C., Ceburnis, D., Arneth, A., Svenningsson, B., Swietlicki, E., Tarozzi, L., Decesari, S., Sonntag, A., Birmili, W., Wiedensohler, A., Boulon, J., Sellegri, K., Laj, P., Baltensperger, U., Laaksonen, A., Joutsensaari, J., Petäjä, T., Kerminen, V.-M., and Kulmala, M.: EUCAARI ion spectrometer measurements at 12 European sites – analysis of new particle formation events, *Atmos. Chem. Phys.*, 10, 7907–7927, doi:10.5194/acp-10-7907-2010, 2010. 8256, 8258, 8268

Metzger, A., Verheggen, B., Dommen, J., Duplissy, J., Prevot, A. S., Weingartner, E., Riipinen, I., Kulmala, M., V. S. D., Carslaw, K. S., and Baltensperger, U.: Evidence for the role of organics in aerosol particle formation under atmospheric conditions, *P. Natl. Acad. Sci. USA*, 107, 6646–6651, doi:10.1073/pnas.0911330107, 2010. 8258

Mirme, A., Tamm, A., Mordas, G., Vana, M., Uin, J., Mirme, S., Bernotas, T., Laakso, L., Hirsikko, A., and Kulmala, M.: A wide range multi-channel Air Ion Spectrometer., *Bor. Env. Res.*, 12, 247–264, 2007. 8253

Mirme, S., Mirme, A., Minikin, A., Petzold, A., Hörrak, U., Kerminen, V.-M., and Kulmala, M.: Atmospheric sub-3 nm particles at high altitudes, *Atmos. Chem. Phys.*, 10, 437–451, doi:10.5194/acp-10-437-2010, 2010. 8251

Nieminen, T., Paasonen, P., Manninen, H. E., Kerminen, V.-M., and Kulmala, M.: Parameterization of ion-induced nucleation rates based on ambient observations, *Atmos. Chem. Phys. Discuss.*, 10, 21697–21720, doi:10.5194/acpd-10-21697-2010, 2010. 8274

Nilsson, E. D. and Kulmala, M.: The potential for atmospheric mixing processes to enhance the binary nucleation rate, *J. Geophys. Res.*, 103(D1), 1381–1389 doi:10.1029/97JD02629, 1998. 8251

Nilsson, E. D., Rannik, U., Kulmala, M., Buzorius, G., and O'Dowd, C. D.: Effects of continental boundary layer evolution, convection, turbulence and entrainment, on aerosol formation, *Tellus B*, 53B, 441–461, 2001. 8251

Nishita, C., Osada, K., Kido, M., and Matsunaga, K.: Nucleation mode particles in upslope valley winds at Mount Norikura, Japan: Implications for the vertical extent of new particle formation events in the lower troposphere, *J. Geophys. Res.*, 113, D06 202, 2008. 8257

Petäjä, T., Mauldin III, R. L., Kosciuch, E., McGrath, J., Nieminen, T., Paasonen, P., Boy, M.,

- Adamov, A., Kotiaho, T., and Kulmala, M.: Sulfuric acid and OH concentrations in a boreal forest site, *Atmos. Chem. Phys.*, 9, 7435–7448, doi:10.5194/acp-9-7435-2009, 2009. 8258
- Shaw, G. E.: Aerosols at a mountain top observatory in Arizona, *J. Geophys. Res.*, 112, D07206, doi:10.1029/2005JD006893, 2007. 8257
- 5 Stratmann, F., Siebert, H., Spindler, G., Wehner, B., Althausen, D., Heintzenberg, J., Hellmuth, O., Rinke, R., Schmieder, U., Seidel, C., Tuch, T., Uhrner, U., Wiedensohler, A., Wandinger, U., Wendisch, M., Schell, D., and Stohl, A.: New-particle formation events in a continental boundary layer: first results from the SATURN experiment, *Atmos. Chem. Phys.*, 3, 1445–1459, doi:10.5194/acp-3-1445-2003, 2003. 8251
- 10 Tammet, H. and Kulmala, M.: Simulation tool for atmospheric aerosol nucleation bursts, *J. Aerosol Sci.*, 36, 173–196, 2005. 8257
- Tunved, P., Nilsson, E. D., Hansson, H.-C., Ström, J., Kulmala, M., Aalto, P., and Viisanen, Y.: Aerosol characteristics of air masses in norther Europe: Influences of location, transport, sinks, and sources, *J. Geophys. Res.*, 110, D07201, doi:10.1029/2004JD005085, 2005. 8259
- 15 Venzac, H., Sellegri, K., and Laj, P.: Nucleation events detected at the high altitude site of the Puy de Dôme research station, France, *Bor. Env. Res.*, 12, 345–359, 2007. 8256, 8261, 8263
- Venzac, H., Sellegri, K., Laj, P., Villani, P., Bonasoni, P., Marioni, A., Cristofanelli, P., Calzolari, F., Fuzzi, S., Decesari, S., Facchini, M.-C., Vuillermoz, E., and Verza, G.-P.: High frequency new particle formation in the Himalayas, *P. Natl. Acad. Sci. USA*, 105, 15666–15671, 2008. 8256, 8257, 8260, 8263
- 20 Venzac, H., Sellegri, K., Villani, P., Picard, D., and Laj, P.: Seasonal variation of aerosol size distributions in the free troposphere and residual layer at the puy de Dôme station, France, *Atmos. Chem. Phys.*, 9, 1465–1478, doi:10.5194/acp-9-1465-2009, 2009. 8253
- 25 Wehner, B., Siebert, H., Ansmann, A., Ditas, F., Seifert, P., Stratmann, F., Wiedensohler, A., Apituley, A., Shaw, R. A., Manninen, H. E., and Kulmala, M.: Observations of turbulence-induced new particle formation in the residual layer, *Atmos. Chem. Phys.*, 10, 4319–4330, doi:10.5194/acp-10-4319-2010, 2010. 8251

**Vertical extent of nucleation events**

J. Boulon et al.

Title Page

Abstract

Introduction

Conclusions

References

Tables

Figures

◀

▶

◀

▶

Back

Close

Full Screen / Esc

Printer-friendly Version

Interactive Discussion



## Vertical extent of nucleation events

J. Boulon et al.

Title Page

Abstract

Introduction

Conclusions

References

Tables

Figures

◀

▶

◀

▶

Back

Close

Full Screen / Esc

Printer-friendly Version

Interactive Discussion

**Table 1.** Formation rate calculated from different parametrizations.

ID.	Model	Pearson's $r$
#1	$J_2 = 4.9 \times 10^{-07} \times \text{H}_2\text{SO}_4^{\text{b}}$	-0.0855
#2	$J_2^+ = 1.9 \times 10^{-10} \times N^+ \text{GlobRad}^{2,\text{a}}$	0.1434
#3	$J_2^+ = 6.5 \times 10^{-18} \times N^+ (\text{H}_2\text{SO}_4)^{2,\text{a}}$	-0.1932
#4	$J_2^- = 1.6 \times 10^{-10} \times N^- \text{GlobRad}^{2,\text{a}}$	0.2328
#5	$J_2^- = 6.7 \times 10^{-18} \times N^- (\text{H}_2\text{SO}_4)^{2,\text{a}}$	-0.1877

<sup>a</sup> from Nieminen et al. (2010)<sup>b</sup> from Kerminen et al. (2010)



**Vertical extent of nucleation events**

J. Boulon et al.

Title Page

Abstract

Introduction

Conclusions

References

Tables

Figures

I◀

▶I

◀

▶

Back

Close

Full Screen / Esc

Printer-friendly Version

Interactive Discussion

**Table 3.** Statistical data of nucleation event occurrence.

	PdD & Opme	Only Opme	Only PdD
Nb. events	87	4	70
Frequency	19.9%	0.91%	16.0%

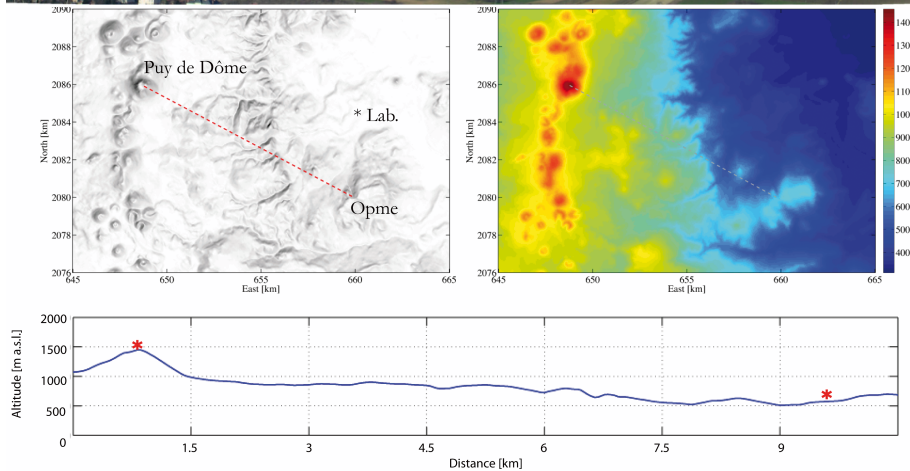


**Fig. 1.** Topographical view of the two measurement sites.

**Vertical extent of nucleation events**

J. Boulon et al.

Title Page

Abstract Introduction

Conclusions References

Tables Figures

◀ ▶

◀ ▶

Back Close

Full Screen / Esc

Printer-friendly Version

Interactive Discussion



## Vertical extent of nucleation events

J. Boulon et al.

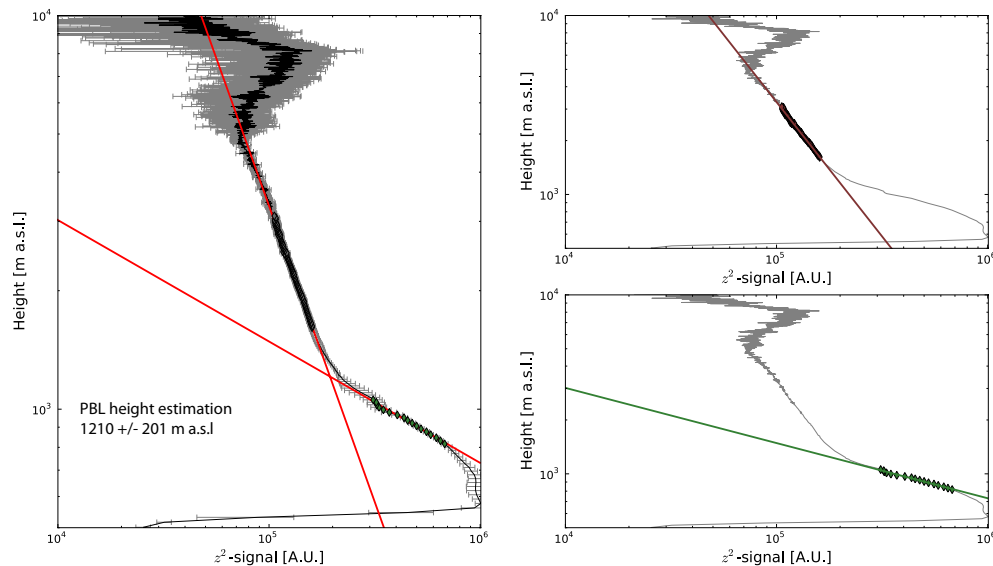
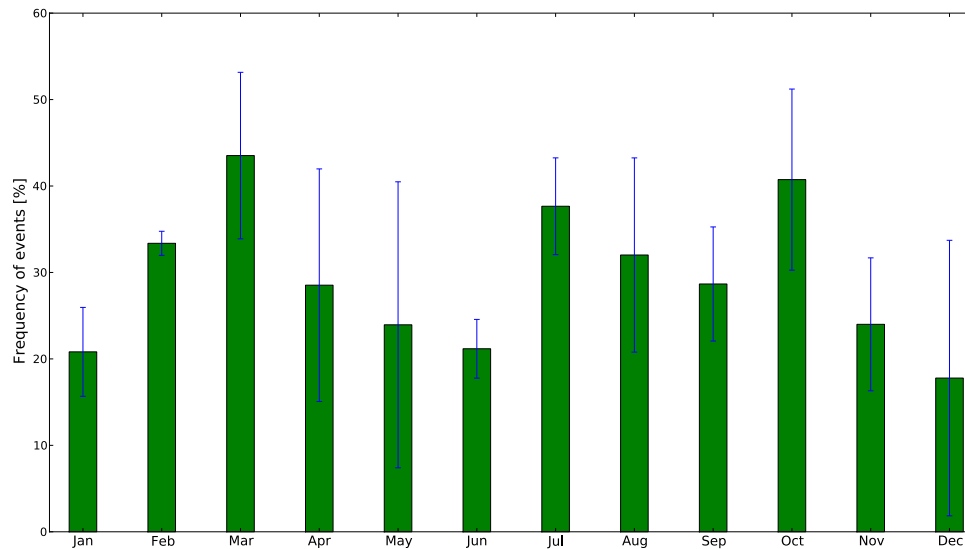


Fig. 2. Method for estimating the PBL and injection layer limits.

[Title Page](#)[Abstract](#)[Introduction](#)[Conclusions](#)[References](#)[Tables](#)[Figures](#)[◀](#)[▶](#)[◀](#)[▶](#)[Back](#)[Close](#)[Full Screen / Esc](#)[Printer-friendly Version](#)[Interactive Discussion](#)

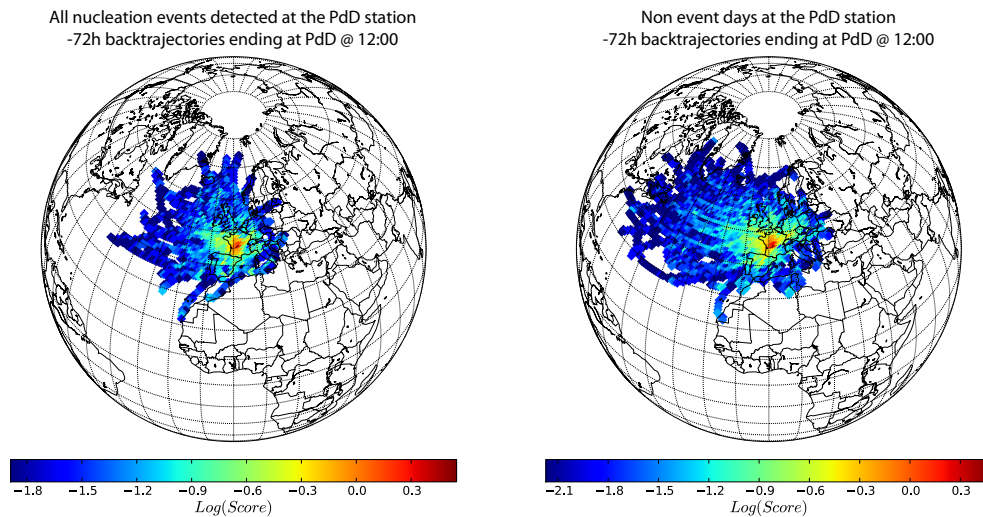
**Vertical extent of nucleation events**

J. Boulon et al.

**Fig. 3.** Monthly mean nucleation frequencies at the puy de Dôme station.[Title Page](#)[Abstract](#)[Introduction](#)[Conclusions](#)[References](#)[Tables](#)[Figures](#)[I◀](#)[▶I](#)[◀](#)[▶](#)[Back](#)[Close](#)[Full Screen / Esc](#)[Printer-friendly Version](#)[Interactive Discussion](#)

**Vertical extent of nucleation events**

J. Boulon et al.

**Fig. 4.** Three days air mass backtrajectories computed with Hysplit model.[Title Page](#)[Abstract](#)[Introduction](#)[Conclusions](#)[References](#)[Tables](#)[Figures](#)[◀](#)[▶](#)[◀](#)[▶](#)[Back](#)[Close](#)[Full Screen / Esc](#)[Printer-friendly Version](#)[Interactive Discussion](#)

## Vertical extent of nucleation events

J. Boulon et al.

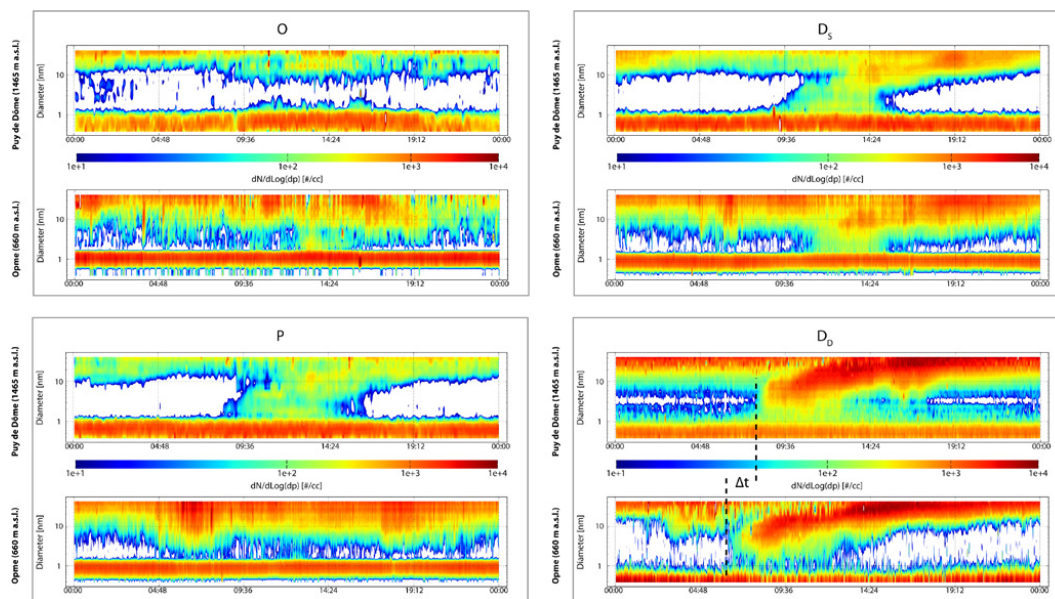


**Fig. 5.** Average temporal evolution of the negatively charged particle size distribution cluster and particle size distributions for the puy de Dôme (upper panels of grey boxes) and Opme (lower panels of grey boxes) in case of “O” events (upper left box), “P” events (lower left box), “D<sub>S</sub>” events (upper right panel) and “D<sub>D</sub>” (lower left box).

Title Page

Abstract

Introduction

Conclusions

References

Tables

Figures

◀

▶

◀

▶

Back

Close

Full Screen / Esc

Printer-friendly Version

Interactive Discussion



## Vertical extent of nucleation events

J. Boulon et al.

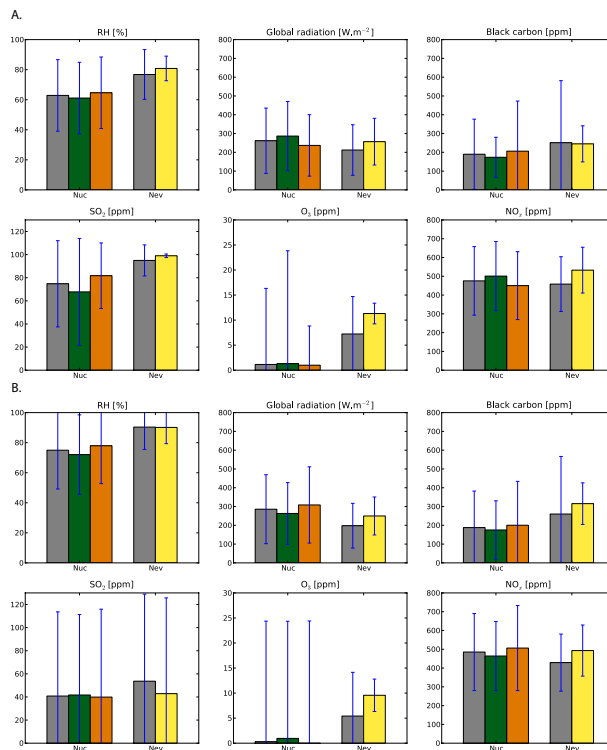


**Fig. 6.** Average and standard deviation of the atmospheric parameters measured at the puy de Dôme station in case of event (Nuc,  $N = 157$ ) or non-event (Nev,  $N = 276$ ) days with or without cloud events filtering (respectively **A** and **B**) calculated over the 09:00–11:00 time period. Grey bars represents the general case, when the nucleation is observed at the puy de Dôme station (Nuc) or not (Nev). The green and the orange bars are respectively for a nucleation events that occur only at the puy de Dôme station ( $N = 70$ ) and an event that occur at both measurement sites ( $N = 87$ ). The yellow bar is for events that only occur at the Opme station ( $N = 4$ ).

Title Page

Abstract

Introduction

Conclusions

References

Tables

Figures

◀

▶

◀

▶

Back

Close

Full Screen / Esc

Printer-friendly Version

Interactive Discussion



## Vertical extent of nucleation events

J. Boulon et al.

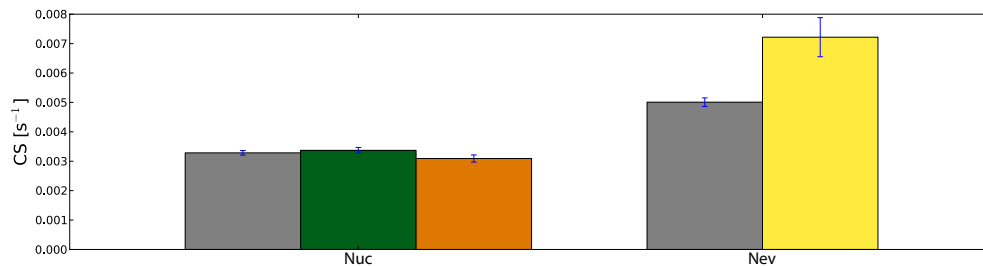


**Fig. 7.** Condensational sink average values for event days (Nuc) and non-event days (Nev) at the puy de Dôme station when  $LWC < 0.02 \text{ g m}^{-3}$ . Grey bars represents the general case, when the nucleation is observed at the puy de Dôme station (Nuc) or not (Nev). The green and the orange bars are respectively for a nucleation events that occur only at the puy de Dôme station ( $N = 70$ ) and an event that occur at both measurement sites ( $N = 87$ ). The yellow bar is for events that only occur at the Opme station ( $N = 4$ ).

[Title Page](#)[Abstract](#)[Introduction](#)[Conclusions](#)[References](#)[Tables](#)[Figures](#)[◀](#)[▶](#)[◀](#)[▶](#)[Back](#)[Close](#)[Full Screen / Esc](#)[Printer-friendly Version](#)[Interactive Discussion](#)

## Vertical extent of nucleation events

J. Boulon et al.

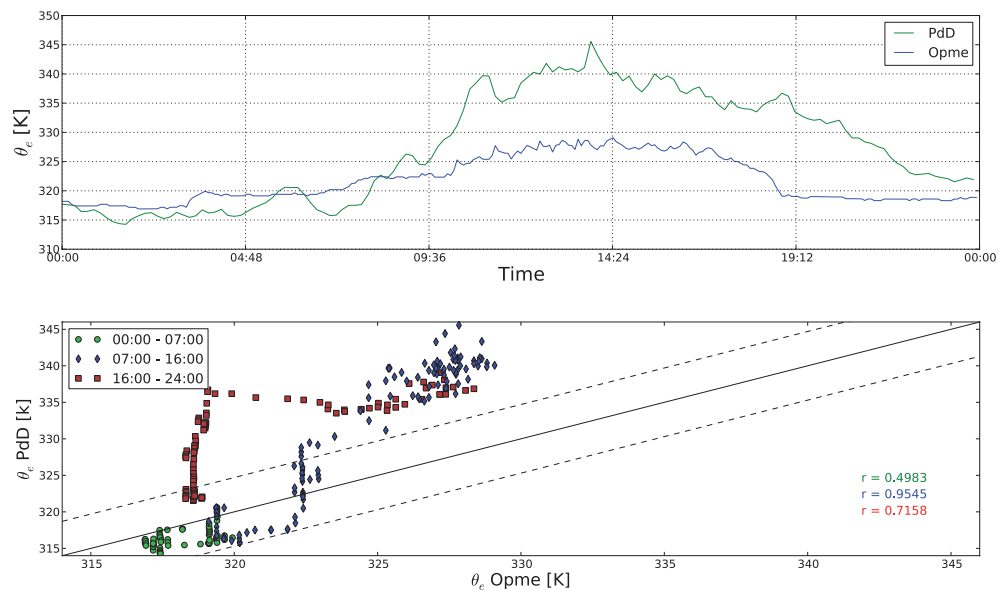


**Fig. 8.** Evolution of equivalent potential temperature,  $\theta_e$  at both sites (upper panel) and the correlation between the two sites (bottom panel) in case of nucleation at Opme site. On the bottom panel, the lines represent the uncertainty boundaries of the  $\theta_e$  (1:1) line.

[Title Page](#)[Abstract](#)[Introduction](#)[Conclusions](#)[References](#)[Tables](#)[Figures](#)[◀](#)[▶](#)[◀](#)[▶](#)[Back](#)[Close](#)[Full Screen / Esc](#)[Printer-friendly Version](#)[Interactive Discussion](#)

## Vertical extent of nucleation events

J. Boulon et al.

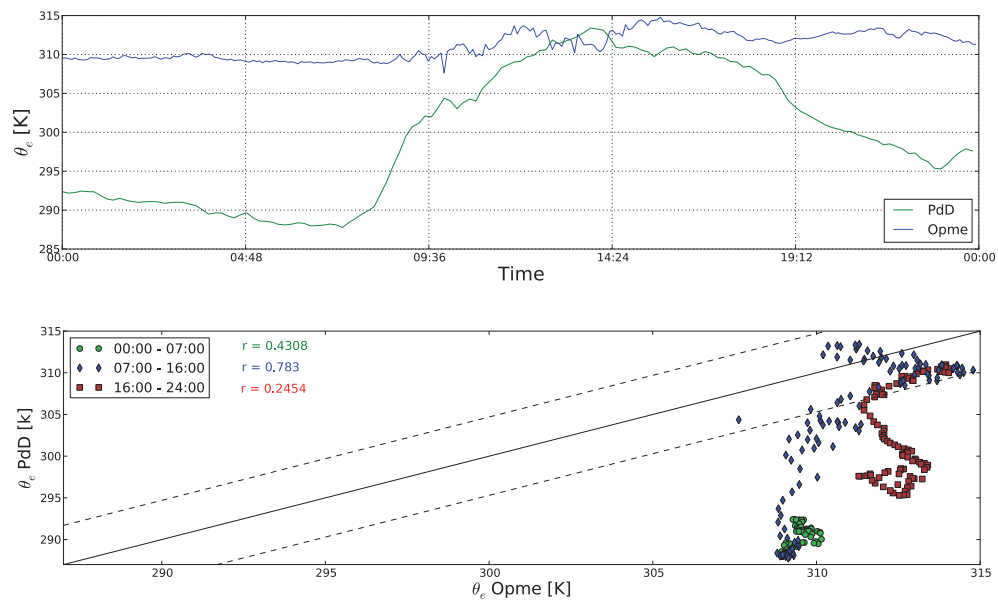


**Fig. 9.** Temporal evolution of equivalent potential temperature at the two instrumented sites during a simultaneous nucleation event.

[Title Page](#)[Abstract](#)[Introduction](#)[Conclusions](#)[References](#)[Tables](#)[Figures](#)[◀](#)[▶](#)[◀](#)[▶](#)[Back](#)[Close](#)[Full Screen / Esc](#)[Printer-friendly Version](#)[Interactive Discussion](#)

Vertical extent of nucleation events

J. Boulon et al.

Title Page

Abstract

Introduction

Conclusions

References

Tables

Figures

◀

▶

◀

▶

Back

Close

Full Screen / Esc

Printer-friendly Version

Interactive Discussion



Discussion Paper | Discussion Paper | Discussion Paper | Discussion Paper | Discussion Paper

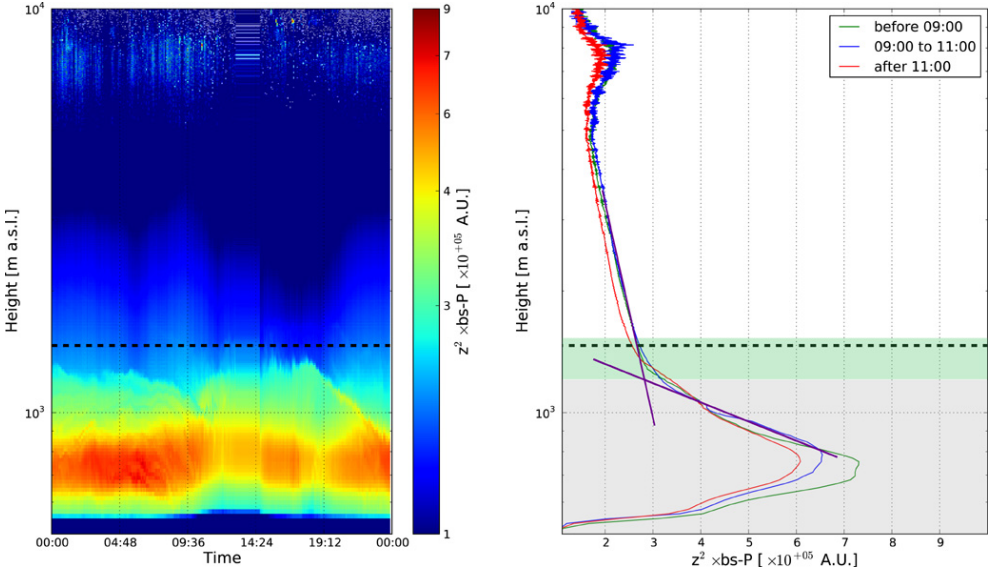


**Fig. 10.** Left panel: LIDAR  $z^2$ -signal evolution in arbitrary units (13 March 2009). Right panel: Average LIDAR  $z^2$ -signal (i) before 09:00 (green line), (ii) between 09:00 and 11:00 (nucleation time) and (iii) after 11:00. On both graphics, the black dot line represents the height of the puy de Dôme station.

## Vertical extent of nucleation events

J. Boulon et al.

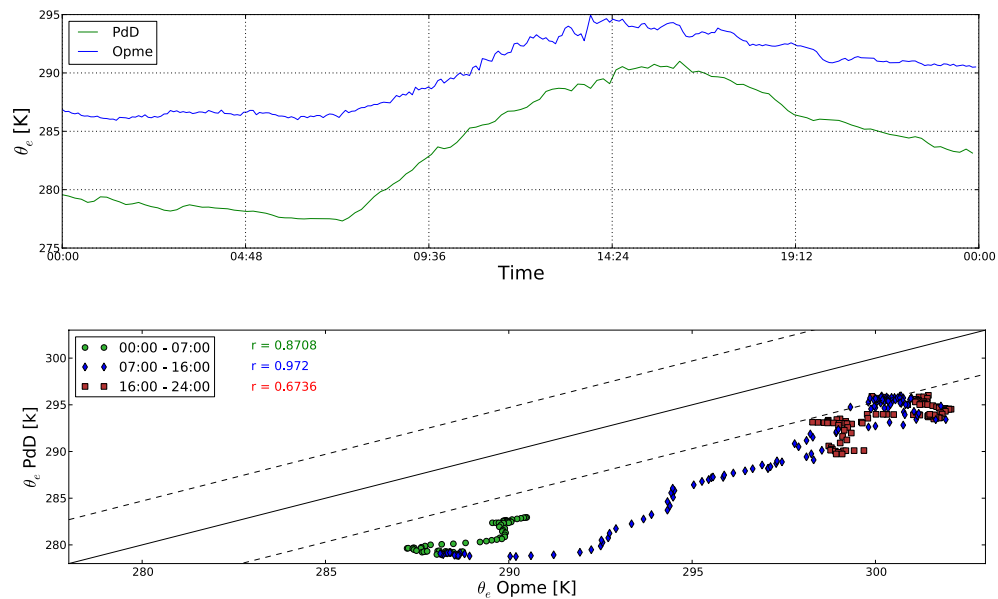


**Fig. 11.** Temporal evolution of equivalent potential temperature at the two instrumented sites during a simultaneous nucleation event, example of the 22 March 2009 event.

[Title Page](#)[Abstract](#)[Introduction](#)[Conclusions](#)[References](#)[Tables](#)[Figures](#)[◀](#)[▶](#)[◀](#)[▶](#)[Back](#)[Close](#)[Full Screen / Esc](#)[Printer-friendly Version](#)[Interactive Discussion](#)

## Vertical extent of nucleation events

J. Boulon et al.

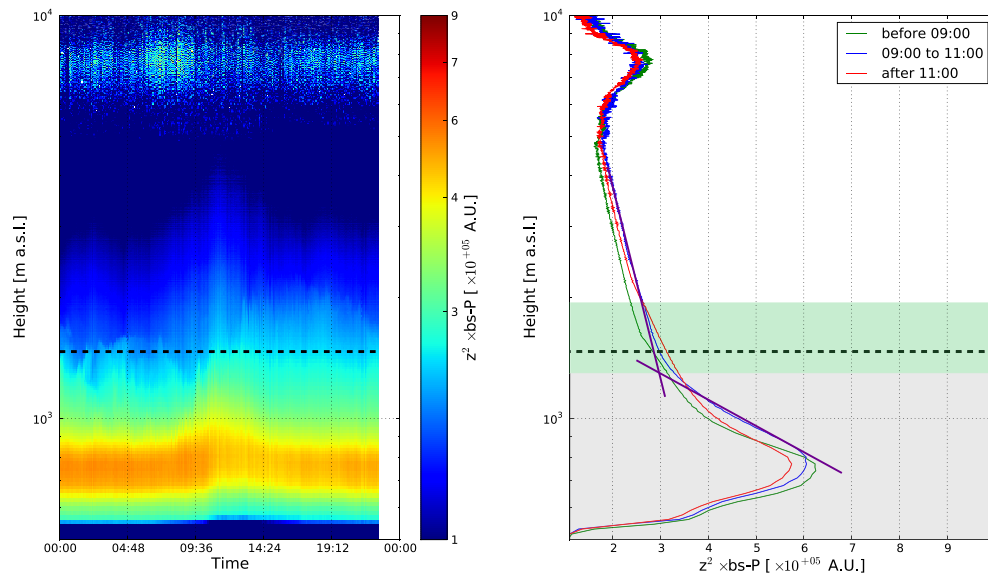


**Fig. 12.** Left panel: LIDAR  $z^2$ -signal evolution in arbitrary units in case of simultaneous nucleation event (22 March 2009). Right panel: Average LIDAR  $z^2$ -signal (i) before 09:00 (green line), (ii) between 09:00 and 11:00 (nucleation time) and (iii) after 11:00. On both graphics, the black dot line represents the height of the puy de Dôme station.

[Title Page](#)
[Abstract](#)
[Introduction](#)
[Conclusions](#)
[References](#)
[Tables](#)
[Figures](#)
[◀](#)
[▶](#)
[◀](#)
[▶](#)
[Back](#)
[Close](#)
[Full Screen / Esc](#)
[Printer-friendly Version](#)
[Interactive Discussion](#)


## Vertical extent of nucleation events

J. Boulon et al.

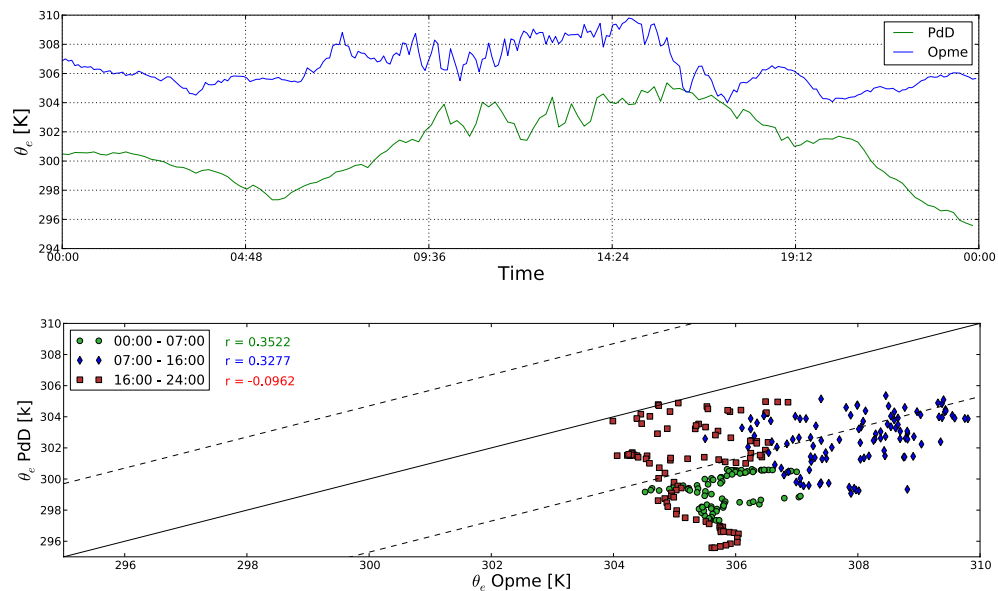


**Fig. 13.** Temporal evolution of equivalent potential temperature at the two instrumented sites during a non-simultaneous nucleation event.

[Title Page](#)[Abstract](#)[Introduction](#)[Conclusions](#)[References](#)[Tables](#)[Figures](#)[◀](#)[▶](#)[◀](#)[▶](#)[Back](#)[Close](#)[Full Screen / Esc](#)[Printer-friendly Version](#)[Interactive Discussion](#)

## Vertical extent of nucleation events

J. Boulon et al.

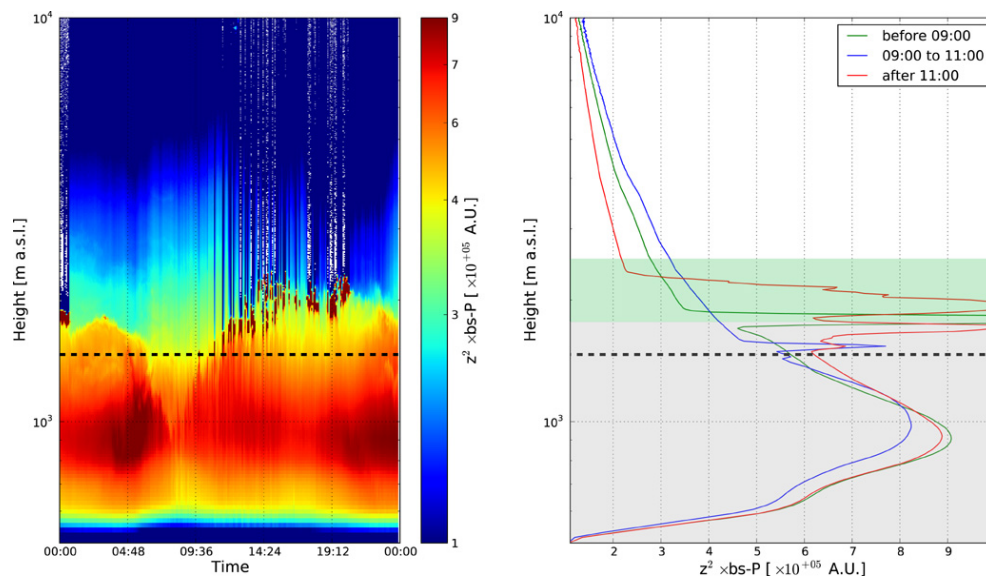


**Fig. 14.** Left panel: LIDAR  $z^2$ -signal evolution in arbitrary units in case of non-simultaneous nucleation event. Right panel: Average LIDAR  $z^2$ -signal (i) before 09:00 (green line), (ii) between 09:00 and 11:00 (nucleation time) and (iii) after 11:00. On both graphics, the black dot line represents the height of the puy de Dôme station.

[Title Page](#)
[Abstract](#)
[Introduction](#)
[Conclusions](#)
[References](#)
[Tables](#)
[Figures](#)
[◀](#)
[▶](#)
[◀](#)
[▶](#)
[Back](#)
[Close](#)
[Full Screen / Esc](#)
[Printer-friendly Version](#)
[Interactive Discussion](#)
